

**“PROPERTIES OF 20% COLD-WORKED 316 STAINLESS STEEL  
IRRADIATED AT LOW DOSE RATE”**

By

T.R. Allen, H. Tsai, J.I. Cole

Nuclear Technology Division  
Argonne National Laboratory-West  
P. O. Box 2528  
Idaho Falls, ID 83403-2528

J. Ohta, K. Dohi, and H. Kusanagi

Central Research Institute of Electric Power Industry  
2-11-1, Iwado Kita, Komae-shi  
Tokyo 201-8511 Japan

The submitted manuscript has been created by the University of Chicago as Operator of Argonne National Laboratory (AArgonne@) under contract No. W-31-109-ENG-38 with the U. S. Department of Energy. The U.S. Government retains for itself, and others acting on its behalf, a paid-up nonexclusive, irrevocable worldwide license in said article to reproduce, prepare derivative works, distribute copies to the public, and perform publicly and display publicly, by or on behalf of the Government.

To be Presented

at

ASTM Radiation Effects on Materials Conferences

Tucson Arizona  
June 18 – 20, 2002

\*Work supported by the U.S. Department of Energy, Office of Nuclear Energy, Science and Technology, under Contract W-31-109-ENG-38.

## **PROPERTIES OF 20% COLD-WORKED 316 STAINLESS STEEL IRRADIATED AT LOW DOSE RATE**

T. R. Allen, Argonne National Laboratory-West  
H. Tsai, Argonne National Laboratory  
J. I. Cole, Argonne National Laboratory-West  
J. Ohta,, Central Research Institute of Electric Power Industry  
K. Dohi, Central Research Institute of Electric Power Industry  
H. Kusanagi,, Central Research Institute of Electric Power Industry

### **Abstract:**

To assess the effects of long-term, low-dose-rate neutron exposure, tensile, hardness, and fracture properties were measured and microstructural characterization performed on irradiated 20% cold-worked Type 316 stainless steel. Samples were prepared from reactor core components retrieved from the EBR-II reactor following final shutdown. Sample locations were chosen to cover a dose range of 1-56 dpa at temperatures from 371-390°C and dose rates from  $0.8\text{-}3.3 \times 10^{-7}$  dpa/s. Irradiation caused hardening, with the ultimate tensile strength (UTS) reaching about 800 MPa near 20 dpa and appearing to saturate at higher doses. The yield strength (YS) follows approximately the same trend as the ultimate tensile strength. At higher dose, the difference between the UTS and YS decreases, suggesting the work-hardening capability of the material is decreasing with increasing dose. The hardness and yield strength increases occur roughly over the same range of dose. While the material retained respectable ductility at 20 dpa, the uniform and total elongation decreased to <1 and <3%, respectively, at 47 dpa. Fracture in the 30 dpa specimen is mainly ductile but with local regions of mixed-mode failure, consisting mainly of dimples and microvoids. The fracture surface of the higher-exposure 47 dpa specimen displays more brittle features. Changes in yield strength predicted from the microstructural components are roughly consistent with the measured changes in yield strength.

### **Introduction**

The objective of this research was to evaluate the effects of long-term, low dose-rate neutron exposure on the swelling, tensile and fracture properties, and the associated microstructural changes in 20% cold worked Type 316 stainless steel. The majority of information available on the effect of radiation on 20% cold-worked Type 316 stainless steel comes from experiments performed in the driver (fueled) regions of the EBR-II reactor where dose rates are on the order of  $1 \times 10^{-6}$  dpa/s (see figure 1). The material analyzed in this study came from 1-mm thick subassemblies (hex cans) irradiated in Row 8 of the reflector region of EBR-II. The displacement rates in row 8 are about an order of magnitude lower than in the fueled region of the core. To examine the effect of dose rate on tensile properties, the results from this study are compared to the results of samples irradiated in Row 2 of EBR-II and reported by Fish et al [1].

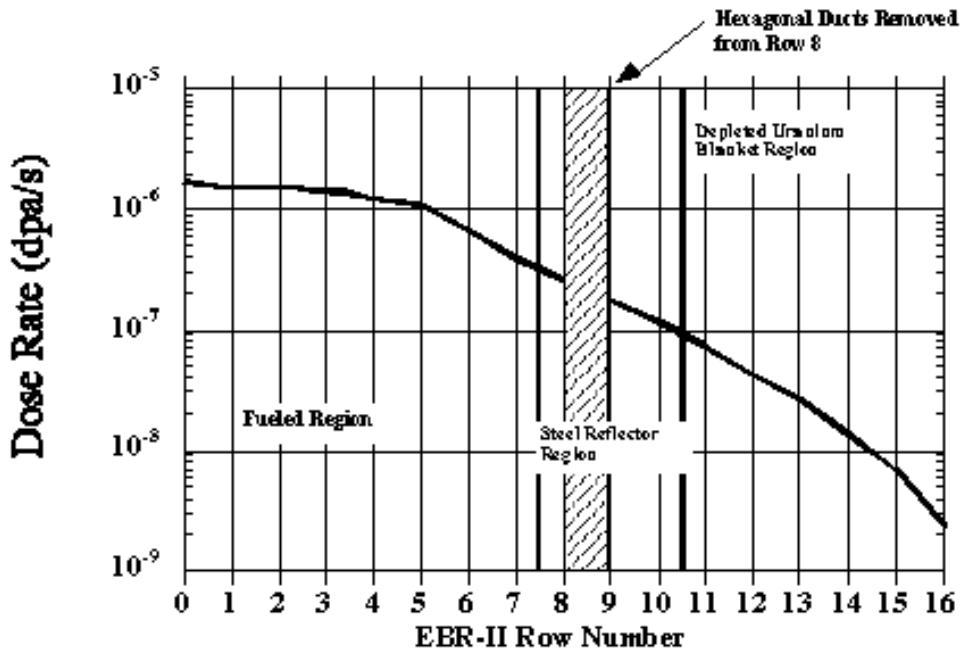


Figure 1 Dose Rate as a function of position at EBR-II core axial midplane

## Experiment

The irradiation conditions for the tensile, hardness, and microstructural samples are listed in Tables 1, 2, and 3.

Samples were taken from two different reflector hex cans removed from EBR-II upon final shutdown. These hex cans were identified as S1951 and S1952. Reflector S1951 was irradiated for 122,000 megawatt-days (MWD) in position 8D6 (row 8) in EBR-II. Reflector S1952 was irradiated for 9525 MWD in position 8A4 (row 8) in EBR-II.

Eight rectangular coupons were prepared by milling from the hex cans at selected locations. The coupons were then machined into tensile specimens using a traveling-wire electric discharge machine. The design of the tensile specimen conforms to both the ASTM-E8 and the Japan Industrial Standard (JIS) specifications for tensile testing. The overall specimen length is 60 mm, with a gauge length of 19 mm and a gauge width of 3.0 mm. The thickness of the specimens is 1.0 mm, corresponding to the thickness of the reflector hex cans. To form a direct comparison with a prior study [1] on irradiated 20 % cold-worked Type 316 stainless steel irradiated at higher dose rate, the strain rate for the present tests was  $4 \times 10^{-5}$ /s, the same as the prior study. From the tensile tests, 0.2% offset yield strength, ultimate tensile strength, uniform elongation and total elongation were derived. Fractography was performed on specimens irradiated to 30 and 47 dpa to determine the effect of irradiation on fracture mode

Vickers hardness was measured using a Nikon QM hardness tester on eight samples. Each sample consists of a 3 mm disk punched from a reflector hex can. The hardness of each of the sample was measured at 25°C and at 370°C. Four indents were made on each sample. The indents were made with a 1000g load.

Transmission electron microscopy samples were made by mechanically punching 1.9cm disks from the hex cans. The 1mm thick 1.9 cm punches were thinned to ~250 microns from which 3 mm disks were punched for transmission electron microscopy studies. Microstructural analysis for samples irradiated to 1, 20 and 30 dpa was carried out in a JEOL 2010 transmission electron microscope (TEM) equipped with an energy dispersive x-ray detector and a scanning transmission electron detector attachment. The microscope was operated at an accelerating voltage of 200 kV.

## Results

Table 1 summarizes the eight tensile tests. Figure 2 displays the measured yield and ultimate tensile strengths as a function of dose. The data indicate hardening with irradiation, with the ultimate tensile strength reaching about 800 MPa near 20 dpa. Beyond that, hardening appears to be saturated. The yield strength also increases with increasing irradiation dose. The narrowing separation between the UTS and YS curves at higher dose suggests the work-hardening capability of the material is decreasing with increasing dose.

Table 1. Summary Engineering Tensile Properties<sup>(1)</sup> for the Eight Tests<sup>(2)</sup>

Specimen	Dose (dpa)	Dose Rate ( $\times 10^{-7}$ dpa/s)	Irrad Temp. (°C)	YS (MPa)	UTS (MPa)	UE (%)	TE (%)
S2T1	1	0.76	371	511	628	10.2	16.5
S2T2	1	0.76	371	473	597	12.0	15.4
S1T1	20	1.2	375	677	810	2.9	5.3
S1T2	20	1.2	375	680	824	3.5	6.6
S1T3	30	1.8	376	767	805	2.3	4.8
S1T4	30	1.8	376	676	805	2.3	5.1
S1T5	47	2.8	385	741	790	0.9	2.8
S1T6	47	2.8	385	770	787	0.5	1.9

(1) YS: 0.2% offset yield strength; UTS: ultimate tensile strength; UE: uniform elongation; and TE: total elongation.

(2) All tests were conducted at a strain rate of  $4 \times 10^{-5}$ /s at a temperature of 370°C.

Ductility of the specimens as a function of dose is shown in figure 3. Both the uniform elongation and total elongation decrease with dose. Unlike the strength data, however, ductility reduction showed no signs of abating at about 20 dpa. While the material retained respectable ductility at near 20 dpa, the uniform and total elongation decreased to <1 and 3%, respectively, at 47 dpa.

Posttest fractography was performed on two representative samples, S1T4 (30 dpa) and S1T5 (47 dpa) using a scanning electron microscope. Necking of the gauge section in the 30 dpa specimen

is evident, but for the higher-dose S1T5 specimen, necking is almost imperceptible. This is consistent with the measured elongation data, which showed further reduction of ductility during irradiation from 30 to 47 dpa. Because necking constitutes a sizable fraction of the gauge deformation after the maximum load (uniform elongation) is attained before fracture, it reflects to a large extent the difference between the uniform and total elongation. In this respect, the differences of 2.8% for the 30-dpa S1T4 and 1.9% for the 47-dpa S1T5 appear to be consistent with the observed necking behavior.

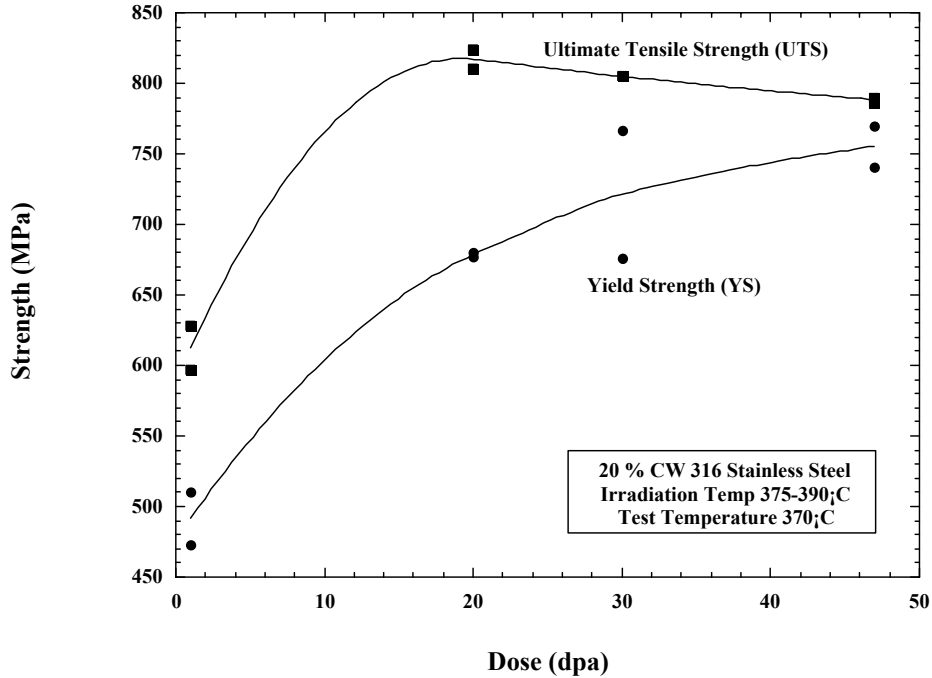


Figure 2 Ultimate tensile strength (UTS) and 0.2% offset yield strength (YS) for 20% cold-worked Type-316 stainless steel hex can duct materials irradiated in EBR-II. The strain rate was  $4 \times 10^{-5}$ /s.

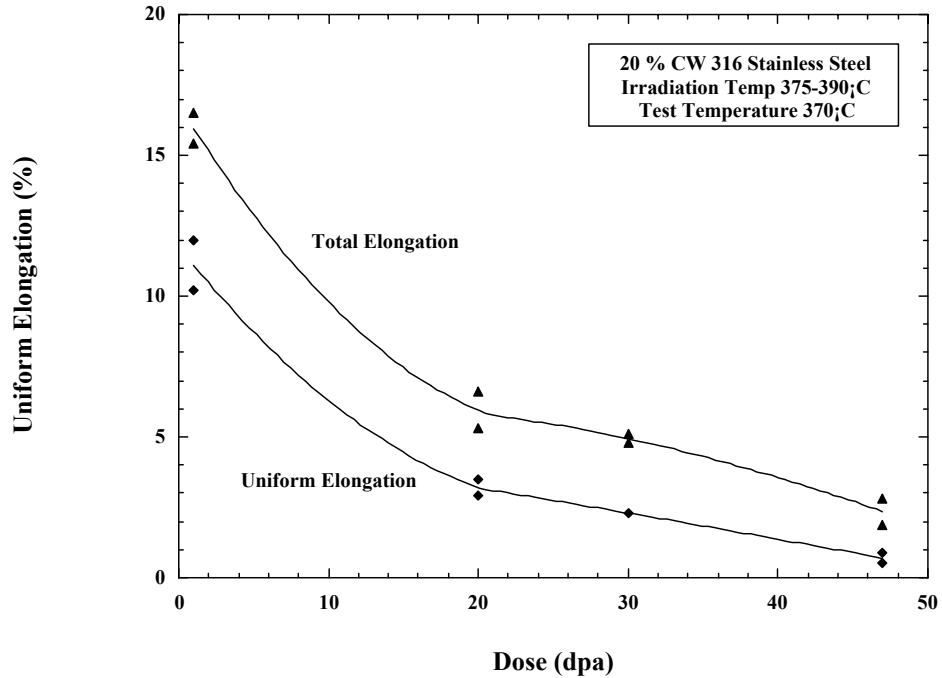


Figure 3 Total and uniform elongation for 20% cold-worked Type-316 stainless steel hex can duct materials irradiated in EBR-II. The strain rate was  $4 \times 10^{-5}$ /s.

Fracture in the 30 dpa specimen is mainly ductile but with local regions of mixed-mode failure. The ductile fracture, illustrated in figure 4, consists mainly of dimples and microvoids. Among the dimples, there are facet features that suggest flow localization and slip band decohesion. The 30 dpa sample has limited areas with mixed mode fracture (not shown) where some failure appears as a transgranular shear along active slip planes. The side surface of the S1T4 specimens shows steps from the tensile deformation; such features are typically associated with dislocation channeling in material.

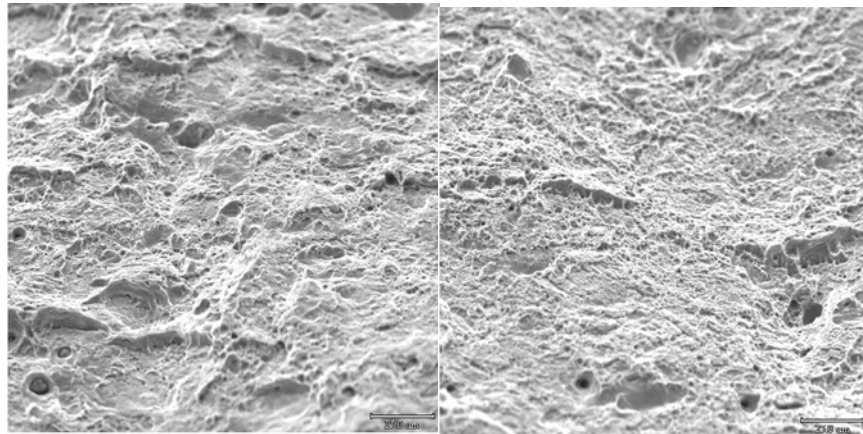


Figure 4 Areas of fracture surface of S1T4 (30 dpa) showing ductile dimples mixed with facets.

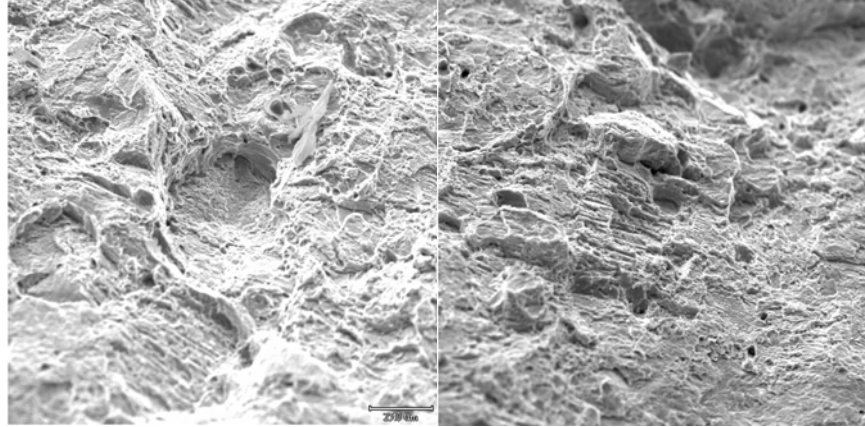


Figure 5. Fracture of the S1T5 (47 dpa) specimen showing channel faceted surface

The fracture surface of the higher-exposure 47 dpa specimen displays significantly more brittle features, as shown in Figure 5. The fracture consists of mainly small facets and slip bands that suggest channel fracture. Dimples and microvoids are far less abundant than in the lower-exposure S1T4 specimen. Noticeable steps are also found on the side surfaces of the specimens.

Table 2 lists the hardness measurements of samples from reflectors S1951 and S1952. Also listed are the punching location, core position, temperature, dose, and dose rate for each sample.

Table 2. Hardness for Samples from Hex Can S1951

Sample ID	Dose (dpa)	Dose Rate ( $\times 10^{-7}$ dpa/s)	Temperature ( $^{\circ}\text{C}$ )	Vickers Hardness (HV) $25^{\circ}\text{C}$	Vickers Hardness (HV) $370^{\circ}\text{C}$
S2P1	1	0.76	373	257 $\pm$ 13	197 $\pm$ 9
S2P2	2	1.5	375	294 $\pm$ 14	199 $\pm$ 9
S1P1	10	0.59	373	330 $\pm$ 17	245 $\pm$ 12
S1P2	15	0.89	374	341 $\pm$ 20	267 $\pm$ 12
S1P3	20	1.2	375	357 $\pm$ 21	273 $\pm$ 14
S1P4	25	1.5	376	367 $\pm$ 20	277 $\pm$ 15
S1P5	30	1.8	379	362 $\pm$ 19	277 $\pm$ 13
S1P6	56	3.3	385	356 $\pm$ 21	260 $\pm$ 13

A summary of the microstructure for the samples irradiated to 1, 20, and 30 dpa is provided in Table 3. Examination of the microstructure at 1 dpa indicates only minor precipitation and no void formation. The network or line dislocation density is estimated to be  $\sim 2 \times 10^{15} \text{ m}^{-2}$ , close to that measured by Maziasz et al. and Johnson et al. [2-3].

A small population of perfect and faulted loops has also formed at 1 dpa. The loops ranged in size from  $\sim 6$  nm to  $\sim 50$  nm with the average loop diameter being  $\sim 22$  nm. Faulted loops form from the clustering of interstitial atoms and grow in size with increasing dose. When they reach a critical radius, they tend to unfault and become perfect loops. The perfect loops are mobile on the glide plane and can interact with other dislocations to form dislocation networks.

A few larger (> 100nm) precipitates are scattered randomly throughout the grain interiors, and these were identified as  $M_{23}C_6$  and Ti-rich MC in the extraction replicas. Typical compositions of the observed precipitates are listed in Table 4. The grain boundaries in the 1 dpa sample are relatively precipitate free.

Table 3. Cavity, Precipitate, and Dislocation Data for 20% CW Type 316 SS Hexagonal Duct Material

	Voids		Precipitates		Frank Loops		Network Dislocations
Dose	Density, $m^{-3}$	Diameter, nm (range)	Density, $m^{-3}$	Diameter, nm (range)	Density, $m^{-3}$	Diameter, nm (range)	Density, $m^{-2}$
1 dpa	N/A	N/A	$< 1.0 \times 10^{20}$	$> 50$	$6.0 \times 10^{20}$	22(8-51)	$1.5 \times 10^{15}$
20 dpa	$1.2 \times 10^{21}$	9.9 (3-26)	$3.4 \times 10^{21}$	13 (6-33)	$3.4 \times 10^{21}$	26 (9-48)	$2.9 \times 10^{15}$
30 dpa	$1.0 \times 10^{21}$	11.1(2-22)	$7.3 \times 10^{21}$	15 (5-53)	$2.1 \times 10^{21}$	27 (6-54)	$2.0 \times 10^{15}$

Table 4. Typical Precipitate Compositions in the Type 316 SS Hexagonal Duct Material Chemical Composition (Wt%)

Dose	Temp	Si	Ti	Cr	Mn	Fe	Ni	Mo	Phase
1 dpa	373°C	0.1	0.0	68.5	1.03	16.2	2.2	12.0	$M_{23}C_6$
		0.2	84.2	8.3	0.0	3.4	0.0	4.5	TiC
20 dpa	375°C	0.56	0.0	66.36	1.13	15.94	2.68	13.32	$M_{23}C_6$
		8.4	0.0	40.3	1.8	17.2	27.5	4.9	$M_6C(\eta)$
30 dpa	379°C	1.11	0.0	53.07	1.25	26.92	4.9	12.75	$M_{23}C_6$
		12.92	0.0	36.21	0.77	19.22	27.48	1.66	$M_6C(\eta)$

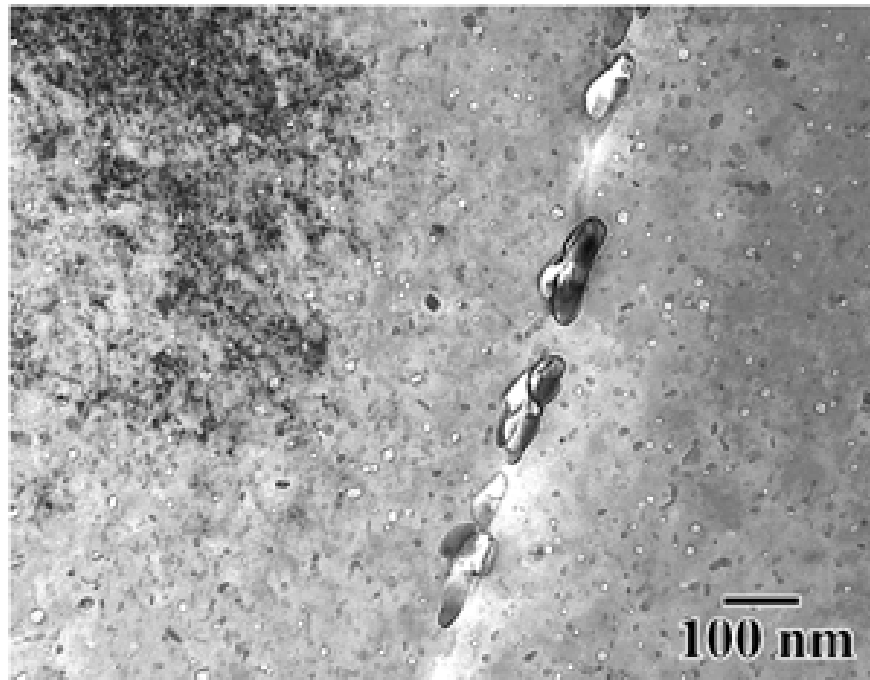


Figure 6. Grain boundary precipitates in 316 SS hex duct irradiated to 20 dpa.

Irradiation to 20 dpa led to the formation of a high density of cavities, dislocations and precipitates. The density of cavities in the 20 dpa sample was on the order of  $1.2 \times 10^{21} \text{ m}^{-3}$  with an average cavity diameter of 9.9 nm. Faceting of the cavities with increasing size is an indication of a transition from gas stabilized bubbles to vacancy driven void growth [4].

The density of matrix precipitates is about three times that of the voids, and the precipitates range in size from about 5 nm up to 50 nm. The high density of precipitates less than 10 nm in size were identified as  $\text{M}_6\text{C}$  type (Ni and Si rich), while larger precipitates ( $> 50 \text{ nm}$ ) were identified as Cr-rich  $\text{M}_{23}\text{C}_6$  type. Additionally, in the both the 20 and 30 dpa samples, a substantial amount of grain boundary precipitation occurred (Figure 6) with many of the boundaries being continuously decorated with  $\text{M}_{23}\text{C}_6$  type carbides. Unlike observations in Type 316 SS irradiated at higher flux and/or higher temperatures, there was no evidence of  $\gamma'$  precipitation in the Type 316 SS hex ducts [5-6]. Many of the cavities that formed in the material are associated with the precipitates. The development of precipitate cavity associations has been observed in several other studies [7-9] and has been linked to enhanced nucleation of helium bubbles at the precipitate interface. The density of precipitates doubles from 20 to 30 dpa with the concentration of the precipitates having greater Ni and Fe concentration at the higher dose. Since greater bulk Ni concentration is known to reduce swelling [10], removing the Ni from the matrix in the form of precipitates should correspond with greater swelling.

Dislocation loops, the majority of which are of the Frank type ( $1/3 \langle 111 \rangle$ ) are seen to populate the microstructure along with a high density of network dislocations. The number density of perfect loops has decreased from what was observed in the 1 dpa sample. The network dislocation density is about a factor of two greater than the 1 dpa sample, suggesting that dislocation loop growth and unfauling has occurred. Loop diameters range from approximately 6 to 50 nm with the average being around 27 nm.

Further irradiation to 30 dpa did not result in a substantial change of the microstructure. Both the void density and void diameter were similar to the 20 dpa sample as well as the dislocation loop density and diameter. The microstructure indicates that the transient regime for swelling extends to a dose greater than 30 dpa, and the increasing precipitate density with dose suggests the changing matrix composition plays an important role in the onset of the 1%/dpa steady-state swelling level.

## **Discussion**

Figure 7 compares the 370°C hardness tests to the yield strength. The increase in hardness and yield strength appear to occur roughly over the same range of dose.

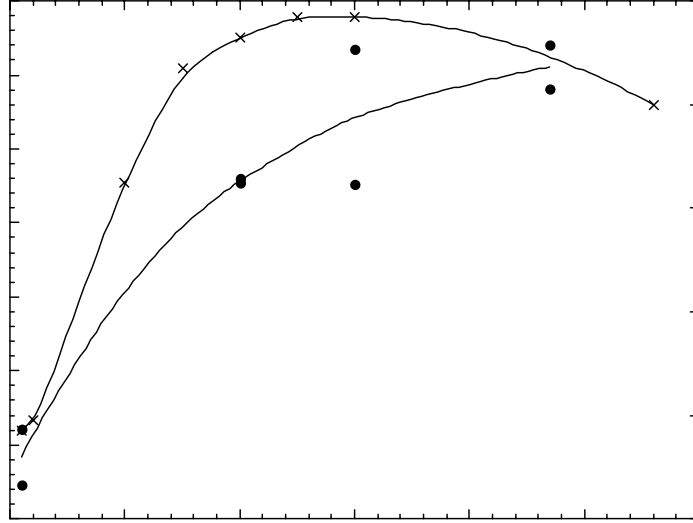


Figure 7. Comparison of hardness and yield strength as a function of dose.

Few studies have attempted to determine the effect of dose rate on mechanical properties. Brager et al. examined the effect of displacement rate on tensile properties of annealed Type 316 stainless steel [11]. For samples irradiated from 371-424°C with a dose rate range of 0.8-8.4x10<sup>7</sup> dpa/s and tensile tested at 385°C, no effect of dose rate on yield strength was noted. A French study on solution annealed Type 316 stainless steel fuel cladding irradiated in the Rapsodie and Phenix reactors indicated that the saturation yield stress was greater in material irradiated in Phenix. The material irradiated in Phenix was irradiated at twice the dose rate of material irradiated in Rapsodie [12]. The two studies found differing results with respect to dose rate effects.

The tensile properties for the samples tested in this study can be compared to those of 20% CW Type 316 stainless steel irradiated in the high dose rate regions of EBR-II. Fish et al., measured the tensile properties of 20% CW Type 316 irradiated in row 2 of EBR-II [1, 13-14]. The dose rate in row 2 is approximately an order of magnitude larger than that of row 8.

Lucas [15] has noted the following relationship between uniform elongation, yield strength, and ultimate tensile strength:

$$\epsilon_u = 0.5 \left( 1 - \frac{\sigma_y}{\sigma_u} \right) \quad (1)$$

Figure 8. displays the hardening  $\left( 1 - \frac{\sigma_y}{\sigma_u} \right)$  as a function of dose. The higher dose rate row 2 samples lose work hardening capability faster than the lower dose rate row 8 samples, even though

there was no significant difference in the uniform elongation. Although no microstructural or fractography data is available from the Fish study, the loss of work hardening capacity may correspond with establishment of dislocation channeling as the primary deformation mechanism. If dislocations are free to travel through the material in slip bands, then less work hardening will occur.

The change in yield strength from microstructural obstacles (dislocation loops, voids, and precipitates) can be estimated from dispersed hardening theory [15]. The change in yield strength due to discrete obstacles is given by:

$$\Delta\sigma_y = M\alpha\mu b\sqrt{Nd} \quad (14)$$

where M relates the shear stresses on a slip plane in a single crystal to the applied tensile stress necessary to activate slip in a polycrystal,  $\alpha$  is the barrier strength,  $\mu$  is the shear modulus of the matrix, b is the Burgers vector of a moving dislocation, N is the number density, and d the average diameter. The inverse of the quantity  $\sqrt{Nd}$  represents average obstacle spacing.

For dislocations, the yield strength increment is given by:

$$\Delta\sigma_y = M\alpha\mu b\sqrt{\rho_d} \quad (15)$$

where  $\rho_d$  is the dislocation density (line length per unit volume). In cold-worked material, the initial yield strength includes a component due to dislocations and therefore during the irradiation, the yield strength increment due to dislocations can either increase or decrease the total yield strength.

The increment in yield strength due to loops, voids, and loops plus voids can be calculated and compared to the measured yield strength. The sum of the microstructural contribution was calculated using a root-mean-square summation:

$$(\Delta\sigma_y = \Delta\sigma_y^{\text{dislocations}} + \sqrt{(\Delta\sigma_y^{\text{voids}})^2 + (\Delta\sigma_y^{\text{loops}})^2} (\Delta\sigma_y^{\text{precipitates}})^2) \quad (16)$$

The values of  $\alpha$  and  $\mu$  used to calculate the yield strength increment are taken from Reference [15] and listed in Table 5. The values of M and b used to calculate the yield strength increment are taken from Reference [16] and are also listed in Table 5. The unirradiated yield strength for 20% cold-worked Type 316 stainless steel tested at 370°C used in calculating the data in Figure 9 is 580MPa [1]. The estimated dislocation density for 20% cold-worked Type 316 stainless steel is  $3 \times 10^{15} \text{ cm}^{-2}$  [16]. Figure 9 indicates that the changes in measured yield strength generally track the changes in yield strength calculated from the microstructure using the inputs from Table 23.

Table 5. Constants for Yield Strength Increment Calculations

Parameter	Precipitates	Dislocations	Voids	Loops
M	3	3	3	3
$\alpha$	0.33	0.11	1	0.33
$\mu$	$6.7 \times 10^{10} \text{ Pa}$			
b	$2.5 \times 10^{-10} \text{ m}$			

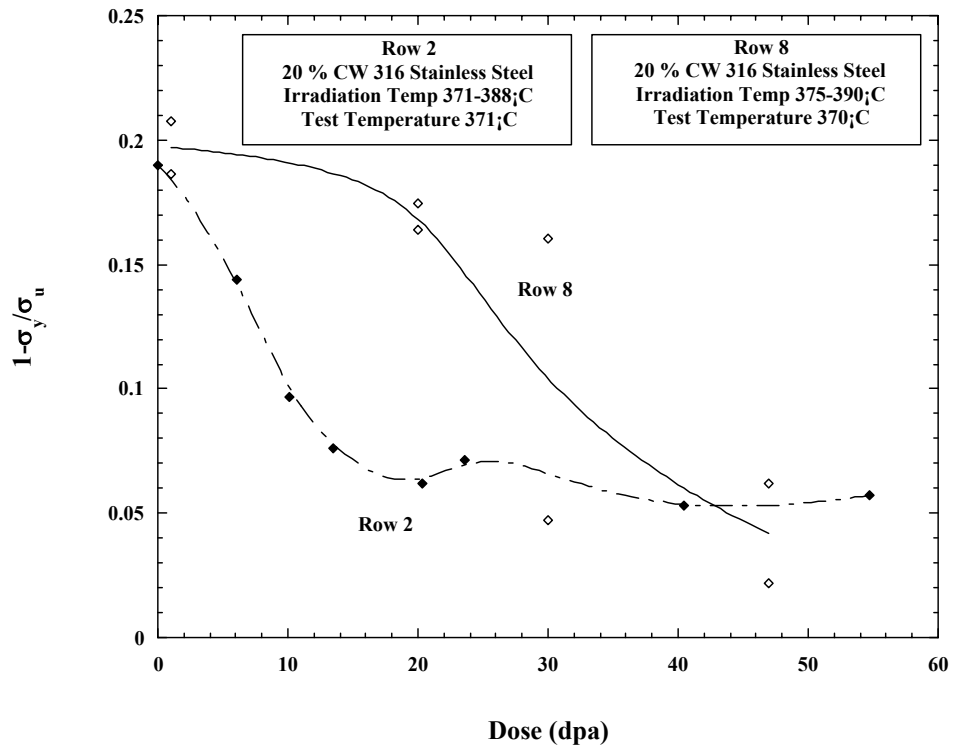


Figure 8 Hardening as a function of dose. The higher dose rate row 2 samples lose work hardening capability faster.

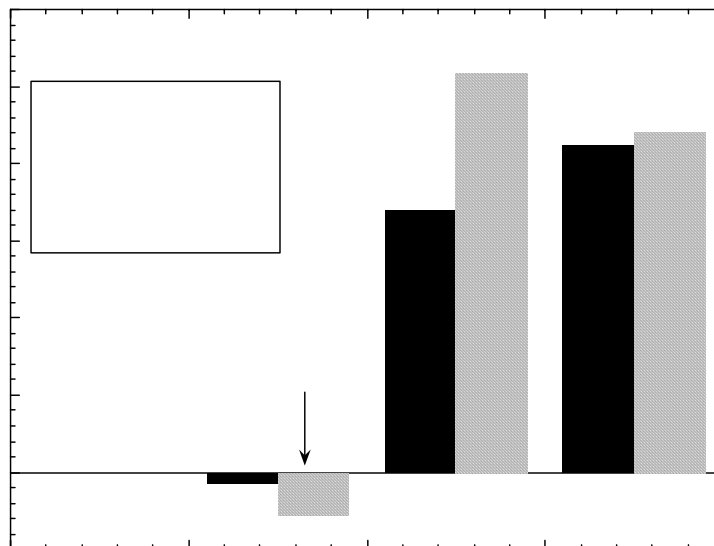


Figure 9 Comparison of increase in yield strength and increase in yield strength estimated from microstructural features.

## Conclusion

The comparison of the strength and elongation of 20% cold-worked Type 316 stainless steel irradiated at different dose rates in EBR-II indicates the following:

- The increases in strength of the row 8 and Row 2 samples follow a similar trend.
- No significant difference in uniform elongation is seen between the row 8 and row 2 samples.
- The higher dose rate row 2 samples lose work hardening capability faster than the lower dose rate row 8 samples.

The elongation and fractography data from the row 8 samples indicate that between 30 and 47 dpa, the fracture mode begins to transition from primarily ductile fracture to a fracture that is more channeled.

## Acknowledgments

The authors gratefully acknowledge the efforts of M. E. Vaughn, J. P. Webb, E. L. Wood, and the staffs at the Hot Fuels Examination Facility at ANL-West. Thanks to K. A. Bunde for performing dose calculations and to R. T. Jensen for performing temperature calculations. Work supported under contract W-31-109-Eng-38 with the Department of Energy.

## References

- [1] R. L. Fish, N. S. Cannon and G. L. Wire, ASTM STP 683, 1979, p. 450.
- [2] P. J. Maziasz, J. A. Horak and B. L. Cox, in Phase Stability During Irradiation, edited by J. R. Holland, L. K. Mansur and D. I. Potter, The Metallurgical Society of AIME, Warrendale, PA 1981.
- [3] Johnson, G. D., Garner, F. A, Brager, H. R., and Fish, R. L., Effects of Radiation on Materials: Tenth conference, ASTM STP 725, D. Kramer, H. R. Brager, and J. S. Perrin, Eds., American Society for Testing and Materials, 1981, pp. 393-412.
- [4] P. J. Maziasz and C. J. McHargue, Int. Mat. Rev., **32 (4)** (1987). p. 190
- [5] W. J. S. Yang, in Radiation-Induced Changes in Microstructure: 13th International Symposium, ed. F. A. Garner, N. H. Packan, and A. S. Kumar. (ASTM, 1987)) p. 628.
- [6] E. H. Lee and L. K. Mansur, J. Nucl. Mat., **278**, (2000) pp. 20-29.
- [7] G. Schoeck, J. App. Phys., **33** (1962) pp. 1745-1747
- [8] D. F. Pedraza and P. J. Maziasz, in Radiation-Induced Changes in Microstructure: 13th International Symposium, ed. F. A. Garner, N. H. Packan, and A. S. Kumar. (ASTM, 1987)) p. 161.
- [9] H. R. Brager and F. A. Garner, in Effects of Radiation on Structural Materials, ed. J. A. Sprague, and D. Kramer, (ASTM, 1979)) p. 207.
- [10] F. A. Garner, in Materials Science and Technology: Nuclear Materials, Vol. 10, edited by B. R. T. Frost (VCH, New York, 1993) p. 422.

- [11] H. R. Brager, L. D. Blackburn, and D. L. Greenslade, *J. Nucl. Mater.*, 122/123 (1984) 332-337.
- [12] J. M. Dupouy, J. Erler, and R. Huillery, *Proceedings of the International Conference on Radiation Effects in Breeder Reactor Structural Materials*, American Institute of Mining, Metallurgical, and Petroleum engineers, 1977, p. 83.
- [13] R.L. Fish, "Tensile Properties of 20% C.W. Type 316 Stainless Steel Irradiated to  $6.0 \times 10^{22}$  n/cm<sup>2</sup> (E>0.1 MeV)," Hanford Engineering Development Laboratory, TC-675-4, 1977, Vol. 1, pp. 1-1 through 1-16.
- [14] R.L. Fish, "Tensile Properties of Irradiated 20% Cold-Worked. AISI 316," Hanford Engineering Development Laboratory, TC-160-5, 1977, pp. 337-344.
- [15] G. E. Lucas, *J. Nucl. Mat.* **206** (1993) 287-305.
- [16] F. Garner, M. Hamilton, N. Panayotou, and G. Johnson, *J. Nucl. Mater.* 103/104 (1981) 803.